Accuracy of Six Degree of Freedom Joint Kinematics and Kinetic Measures During Normal and Pathological Gait: A Simulation Study

By

Anne Schmitz (nee Baus)

A thesis submitted in partial fulfillment of

the requirements for the degree of

Master of Science

Biomedical Engineering

At the

University of Wisconsin-Madison

2008

Acknowledgements

This work was funded by the Shriners Hospitals for Children.

I gratefully acknowledge the work of Darryl Thelen, my advisor at UW Madison, Dustin Bruening of Shriners, and Frank Buczek at NIOSH and Shriners.

Table of Contents

List of Figures

List of Tables

Executive Summary[1]

Anne Schmitz[1], Darryl Thelen[1,2,3], Dustin Bruening[4], Frank Buczek[4,5]

Departments of [1]Biomedical Engineering, [2]Mechanical Engineering, [3]Orthopedics and Rehabilitation, University of Wisconsin-Madison, Madison, WI, USA
[4]Shriners Hospitals for Children, Erie, PA, USA
[5]National Institute for Occupational Safety & Health (NIOSH), Morgantown WV, USA

Introduction

The conventional gait model (CGM) uses a minimal marker configuration to track three-dimensional lower extremity motion[1]. However, the CGM relies on shared markers between segments, which may adversely affect the reliability of non-sagittal joint angles[2]. A number of researchers have opted to use clusters of three or more markers on each segment to independently assess all 6 segmental degrees of freedom (DOF)[3]. A prior study by our group showed that gait measures derived using redundant marker sets differ significantly from those obtained using a CGM approach in normal subjects, particularly in the non-sagittal plane[4]. However, it is unknown whether the differences found actually reflect greater accuracy, or whether comparable differences would be observed in pathological gait. The goal of this study was to compare the accuracy of non-sagittal joint kinematics derived from inverse kinematic models based on shared and independent marker sets.

Clinical Significance

Pathological gait often includes substantial non-sagittal motion. However, a lack of confidence in non-sagittal gait measures diminishes the usage of such data for treating movement disorders. The results of this study suggest that use of independent marker sets on each limb may improve the accuracy of transverse plane joint angles, and hence may allow for greater consideration of non-sagittal motion in treatment planning.

Methods

We generated gait simulations of six healthy children (4 males, 2 females; age, 9 ± 1.5 yrs) and two cerebral palsy (CP) patients (1 male age 10 yrs with apparent equinus, 1 female age 14 yrs with Winters type 4 gait pattern) walking over ground at a preferred speed. To generate the simulations, we first scaled a generic three-dimensional, whole body model (with 34 degrees of freedom) to match the measured segment lengths of each subject. We then used a least squares forward dynamics algorithm to compute the pelvic motion and joint angular trajectories over a gait cycle that were optimally consistent with the measured marker kinematics and ground reactions, while also satisfying the overall equations of motion of the system[5]. The results were a set of joint torque-actuated forward dynamic simulations that closely resembled subject-specific gait patterns. Simulated angles were generally within 1 deg of those obtained using more conventional inverse kinematic approaches.

Ideal marker trajectories were then generated assuming that the markers were rigidly fixed to each segment in the simulations. Both random equipment noise (Gaussian noise with 1 mm s.d.) and soft tissue artefact (continuous noise model with random amplitude<10 mm,

[1] This abstract was submitted to the Gait and Clinical Movement Analysis Society Conference on Oct 15, 2008.

frequency f<4 Hz, and phase[6]) were then added to the noise free marker trajectories. We computed the joint angles from both the corrupted marker trajectories using six degree of freedom inverse kinematic analyses with two marker sets: 1) A shared marker set in which a virtual hip joint center, and the lateral knee and ankle markers were shared by both the proximal and distal segments, 2) An independent marker set in which 4 tracking markers on each segment were used to compute 6 dof segmental position. We quantified accuracy as the root-mean-squared (RMS) difference between the reconstructed and actual joint angles over a full gait cycle.

Results

Use of an independent marker set resulted in smaller RMS errors for hip, knee, and ankle internal/external rotation angles, and ankle ab/adduction when compared to a shared marker set (Table 1). However, errors in hip ab/adduction were slightly larger using an independent marker set. Model effects on accuracy were similar whether processing normal or pathological gait.

Discussion

Our results suggest that the use of independent marker sets, in which 3 or more markers are placed on a rigid plate attached mid-segment, may enhance the accuracy of 3D joint angles. The most noteworthy improvements were internal-external rotation angles and likely result from using redundant non-collinear markers displaced from the long axis of the joint. Our analyses considered the effect of equipment noise and soft-tissue artefact. However, implementation also requires consideration of how soft tissue noise can vary systematically with marker placement. We conclude that the development and use of optimized, independent marker sets may enhance the confidence that practitioners have in using non-sagittal biomechanical measures to plan treatment.

Table 1: Root mean square (RMS) errors for non-sagittal joint angles using shared and independent marker sets on each segment.

Variable	Normal		Cerebral Palsy		
	Shared Marker Set	Independent Marker Set	Shared Marker Set	Independent Marker Set	Model Effect Significant?
Hip Ab/adduction	2.6 (0.7)	4.3 (1.0)	1.9 (0.8)	4.9 (0.3)	*
Hip Rotation	7.8 (3.7)	4.8 (1.5)	6.7 (2.1)	4.6 (1.6)	*
Knee Ab/adduction	3.3 (1.2)	4.4 (0.8)	4.9 (1.7)	5.2 (0.8)	
Knee Rotation	18.6 (7.0)	6.5 (1.6)	16.5 (4.1)	5.6 (0.6)	*
Ankle Ab/adduction	7.1 (2.6)	3.4 (0.9)	6.2 (1.3)	4.1 (0.6)	*
Ankle Rotation	16.0 (7.7)	4.8 (0.9)	13.9 (4.4)	4.0 (1.4)	*

References

1. Davis, R.B., et al. (1991) *Human Movement Science* 10, 575-587
2. Leardini, A., et al. (2005) *Gait & Posture* 21, 212-225
3. Cappozzo, A., et al. (1997) *IEEE Trans Biomed Engr* 44, 1165-1174
4. Buczek, F.L., et al. (2005) Gait and Clinical Movement Analysis Society
5. Remy, C.D. and D.G. Thelen (2008) *J Biomech Eng* in press
6. Cheze, L., et al. (1995) *J Biomech* 28, 879-884

Background

Tracking motion with Stereophotogrammetry

The goal of tracking motion with stereophotogrammetry is to collect quantitative data about the underlying musculoskeletal system of a person during movement. For example, data of interest are usually joint kinematics. These analyses require known musculoskeletal geometry and three-dimensional instantaneous position and orientation of the bones during the movement.

A subject specific musculoskeletal model is created using cadaveric data and an upright standing calibration trial where the subject stands still with retro-reflective skin markers on anatomical landmarks and tracking points (Figure 1). The markers give three-dimensional spatial positions and are used to determine the instantaneous position and orientation of the underlying bone during movement.

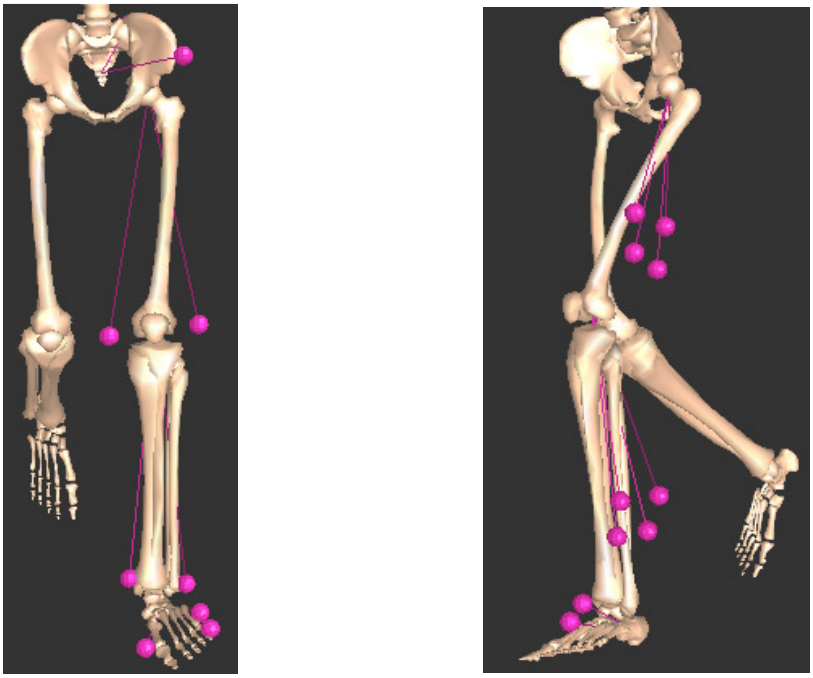

Figure 1: The left figure shows markers placed on palpable anatomical landmarks of the left leg. The right picture shows additional tracking markers on the left leg.

Segment reference frames have a physiological meaning and often approximate the sagittal, frontal, and transverse planes of the bone [7]. For example, the segment coordinate system of the femur is commonly located at the center of the femoral head (Figure 2). This location may be determined from anatomical landmarks on the pelvis [8], functionally during a calibration trial [9-11], or as a transformation of the pelvis reference frame using cadaveric data [12]. The orientations of the axes coincide with the pelvis frame orientation during the static calibration trial. This is beneficial for determining joint angles later.

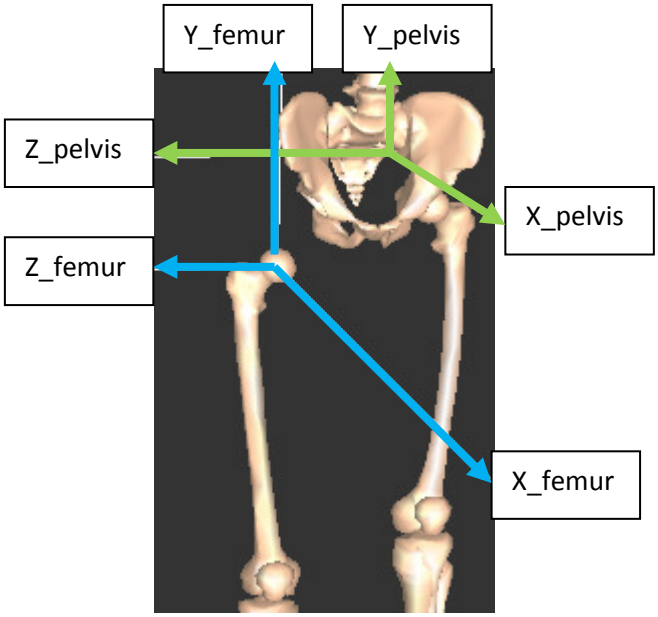

Figure 2: The segment reference frame for the femur is commonly located at the center of the femoral head with the axes defining the sagittal, frontal, and transverse planes of the bone. Picture from [13]

Technical reference frames are calculated from the tracking markers (Figure 3). These frames vary between trials and subjects, since the tracking markers are not always placed in the same location relative to the bone.

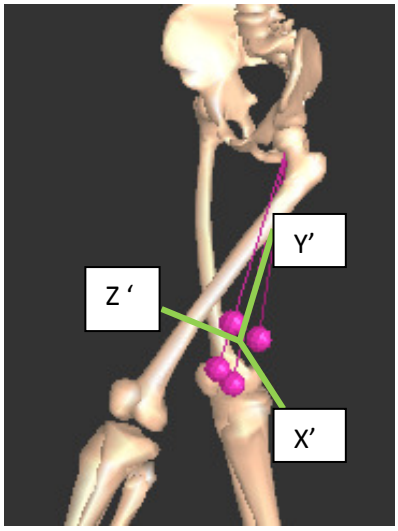

Figure 3: Technical reference frames are calculated from the tracking markers.

During the static calibration trial, the position and orientation of the technical frame relative to the segment frame is calculated. During the motion, anatomical markers are removed and just the tracking markers are used to determine the motion of the underlying bones. The technical frame orientation and position is recalculated at each point in time. Since the relative orientation and position of the technical and segment frames are constant, assuming a rigid bone, the segment frame can also be recalculated at each point in time. Joint kinematics can then be determined by calculating the relative motion between two adjacent segments' reference frames using inverse kinematics, which will be discussed in more detail later.

Cappozzo, Della Croce, Leardini, and Chiari have written excellent reviews on stereophotogrammetry theory [7], errors associated with motion capture [2, 14], and how these errors affect calculated joint kinematics [15]. Davis and Whittle have written articles on clinical gait analysis [16, 17].

Analyzing Motion Capture Data

First, a generic musculoskeletal model is created with virtual markers placed in the same anatomical locations as the experimental markers. This generic model, along with upright calibration data from motion capture, can be used to scale the model to fit a subject. The segments of the generic model are scaled using defined scaling rules, shown in the appendix. Marker locations corresponding to a static pose is computer by averaging marker positions in the static calibration trial. Joint angles that optimally fit the scaled skeleton to the anatomical marker positions measured during calibration are computed. This is the same algorithm used in inverse kinematics. Local coordinates of virtual markers on the scaled model are moved so the global marker positions match identically with experimental marker positions from the calibration trial.

Next, the scaled model and motion capture data (marker positions over time and force plate data) can be used to calculate joint angles that position the model in a pose that best matches the experimental motion data at each time step. This process is called inverse kinematics and considered a weighted least squares problem with the equation of Figure 4.

The weighted least squares problem solved by IK is

$$\min_{\mathbf{q}} \left[\sum_{i \in \text{markers}} w_i \left\| \mathbf{x}_i^{\text{exp}} - \mathbf{x}_i(\mathbf{q}) \right\|^2 + \sum_{j \in \text{unprescribed coords}} \omega_j \left(q_j^{\text{exp}} - q_j \right)^2 \right]$$

$$q_j = q_j^{\text{exp}} \text{ for all prescribed coordinates } j$$

OpenSim User's Guide 1.0, 2008

where $\mathbf{q}$ is the vector of generalized coordinates being solved for, $\mathbf{x_i}^{\text{exp}}$ is the experimental position of marker i, $\mathbf{x_i(q)}$ is the position of the corresponding marker on the model (which depends on the coordinate values), q_j^{exp} is the experimental value for coordinate j.

Figure 4: This is the equation solved during inverse kinematics to find joint angles.

During inverse kinematics, marker errors are introduced. These errors are the differences between experimental marker and model marker positions. Each marker has a weight that controls this error. The

higher the weight, the lower the marker error. Higher weights are assigned to markers trusted to have low placement error, like the pelvis markers. Joint constraints are also assumed during inverse kinematics. For example, the hip is commonly modeled as a ball and socket. The appendix summarizes joint models used for the hip, knee, and ankle, as seen in the literature.

Finally, joint angles from inverse kinematics can be used in inverse dynamics to calculate joint torques and powers. This process is solved using the classical equations of motion, Figure 5.

The classical equations of motion may be written in the following form:

$$\underbrace{\boldsymbol{M}(\boldsymbol{q})\ddot{\boldsymbol{q}} + \boldsymbol{C}(\boldsymbol{q},\dot{\boldsymbol{q}}) + \boldsymbol{G}(\boldsymbol{q})}_{\text{knowns}} = \underbrace{\boldsymbol{\tau}}_{\text{unknowns}}$$

OpenSim User's Guide 1.0, 2008

where N is the number of degrees of freedom; $\boldsymbol{q}, \dot{\boldsymbol{q}}, \ddot{\boldsymbol{q}} \in \boldsymbol{R}^N$ are the vectors of generalized positions, velocities, and accelerations, respectively; $\boldsymbol{M}(\boldsymbol{q}) \in \boldsymbol{R}^{N \times N}$ is the system mass matrix; $\boldsymbol{C}(\boldsymbol{q}, \dot{\boldsymbol{q}}) \in \boldsymbol{R}^N$ is the vector of Coriolis and centrifugal forces; $\boldsymbol{G}(\boldsymbol{q}) \in \boldsymbol{R}^N$ is the vector of gravitational forces; and $\boldsymbol{\tau} \in \boldsymbol{R}^N$ is the vector of generalized forces.

Figure 5: Inverse dynamics is solved using the classical equations of motion.

For more details on analyzing gait using scaling, inverse kinematics, and inverse dynamics, see the OpenSim User's Guide [18]. OpenSim is open source software used to analyze motion capture data.

Introduction

Cerebral palsy is the most common motor disorder originating in childhood [19] and can lead to bone deformities, muscle contractures, and/or joint degeneration if left untreated. Therefore, cerebral palsy is treated at an early age with aggressive surgeries like tendon lengthening, bony fusions, and derotation osteotomies [20]. Choosing a treatment plan is now commonly based on gait analysis, observation, and the physician's experience [19, 21]. However, the outcomes of these procedures are inconsistent at best. Accurate calculations of joint angles, translations, and moments during gait analysis are important to deciding the correct treatment option.

Motion analysis of human walking is widely used for planning and assessing the treatment of movement disorders. However, there is continuing debate about the accuracy of the biomechanical measures obtained using different marker sets and models. The conventional gait model (CGM) uses a minimal marker configuration to track three-dimensional lower extremity motion [1, 22, 23]. CGM remains extremely popular, in part, due to its long history, which enables comparisons with databases of patients. However, potential deficiencies with the CGM arise due to a hierarchical structure in which virtual joint centers at the hip, knee and ankle are shared between adjacent segments. These limitations may adversely affect the reliability of non-sagittal motions in patients with movement disorders [2].

As motion capture technology has steadily improved, a number of researchers have opted to use clusters of three or more physical markers on each segment to independently assess all 6 segmental degrees of freedom (dof) [3, 24, 25]. Six dof models have a potential advantage of being able to account for abnormal joint kinematics, e.g. subluxation. Further, a prior study by our group showed that gait measures derived from 6 dof models differ from those obtained using a CGM approach in normal subjects, particularly in the non-sagittal plane [4]. However, it is challenging to determine whether the

joint translations and differences in non-sagittal rotations actually reflect greater accuracy, since ground truth measures are unknown when processing experimental data.

Synthetic motion data can be used to systematically assess how soft tissue and equipment noise in marker data can alter the accuracy of biomechanical measures. The goal of this study was to use synthetic gait simulations to assess the relative accuracy of three-dimensional kinematics and kinetics derived using shared and independent marker sets. To do this, we first derived forward dynamic simulations of both normal and pathological gait. We then created noise-free marker trajectories that would occur if the linked segment model was a perfect representation of the person. Both systematic and random noise were then added to the marker trajectories. Noise polluted marker trajectories were subsequently processed using models based on shared and independent marker sets. We then tested the hypothesis that the use of independent marker sets on each segment would improve the accuracy of non-sagittal rotations and moments and would provide for more reliable estimates of joint translations, when compared to a shared marker set.

Materials and Methods

Subjects

8 normal subjects (4 males, 4 females; age, 9 ± 2 yrs) and 6 cerebral palsy subjects (5 males, 1 female; age, 12 ± 2 yrs) participated in this study. The cerebral palsy subjects exhibited apparent equinus, crouch gait, Winters type 2, and Winters type 4 gait patterns [26, 27].

Data collection

All subjects walked across a ten meter walkway with force plates near the midpoint of the walkway. Whole body motion was tracked using 86 retro reflective motion capture markers (Figure 6), 42 markers on the upper body and 44 on the lower extremities. On the lower extremities, 22 markers were placed on anatomical landmarks and 22 were used to enhance segment tracking and reduce soft tissue artifact [3]. The tracking markers were fixed to plastic plates held in place with elastic wrap. Using a ten-camera Vicon 612 system (VICON, Oxford Metrics, Oxford, U.K.), kinematic data were collected at 120 Hz. Ground reaction forces were synchronously recorded at 1560 Hz using three AMTI OR6-7 force plates (Advanced Mechanical Technology, Inc, Watertown, MA, USA).

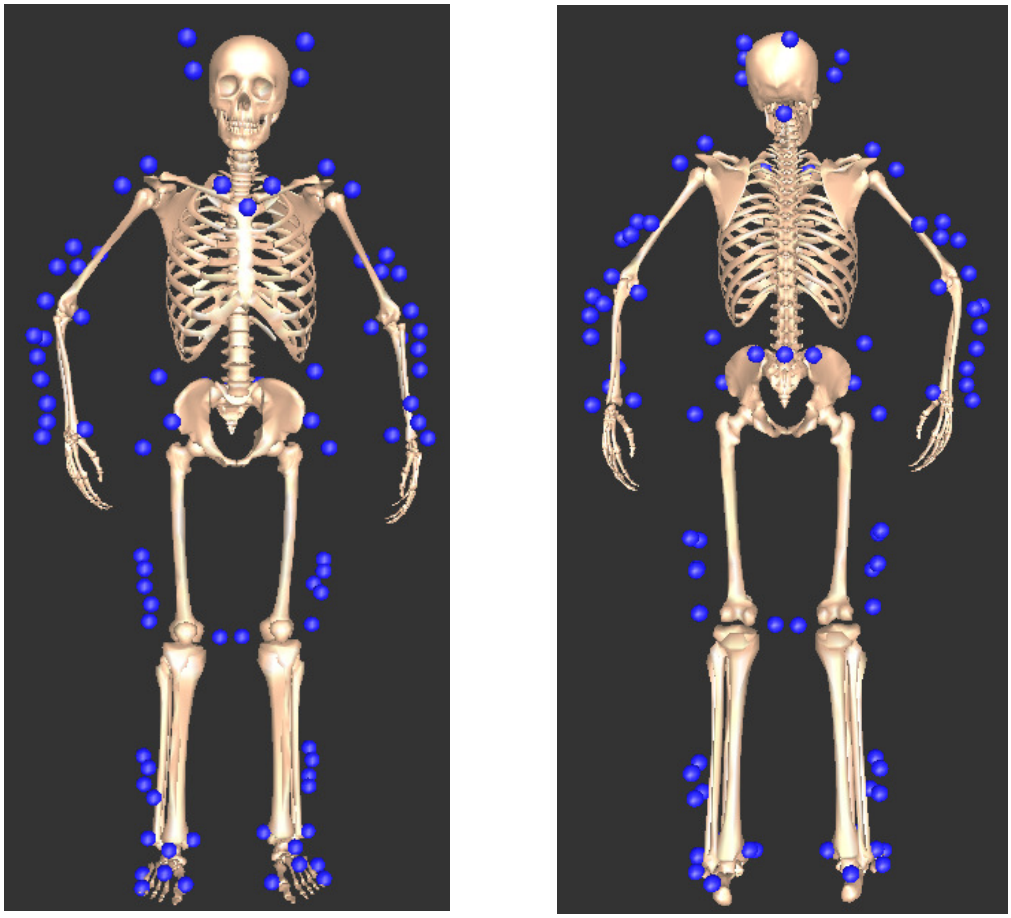

Figure 6: 86 retro reflective motion capture markers were used to track whole body motion: 42 markers on the upper body and 44 on the lower extremities.

Simulation *(Figure 7)*

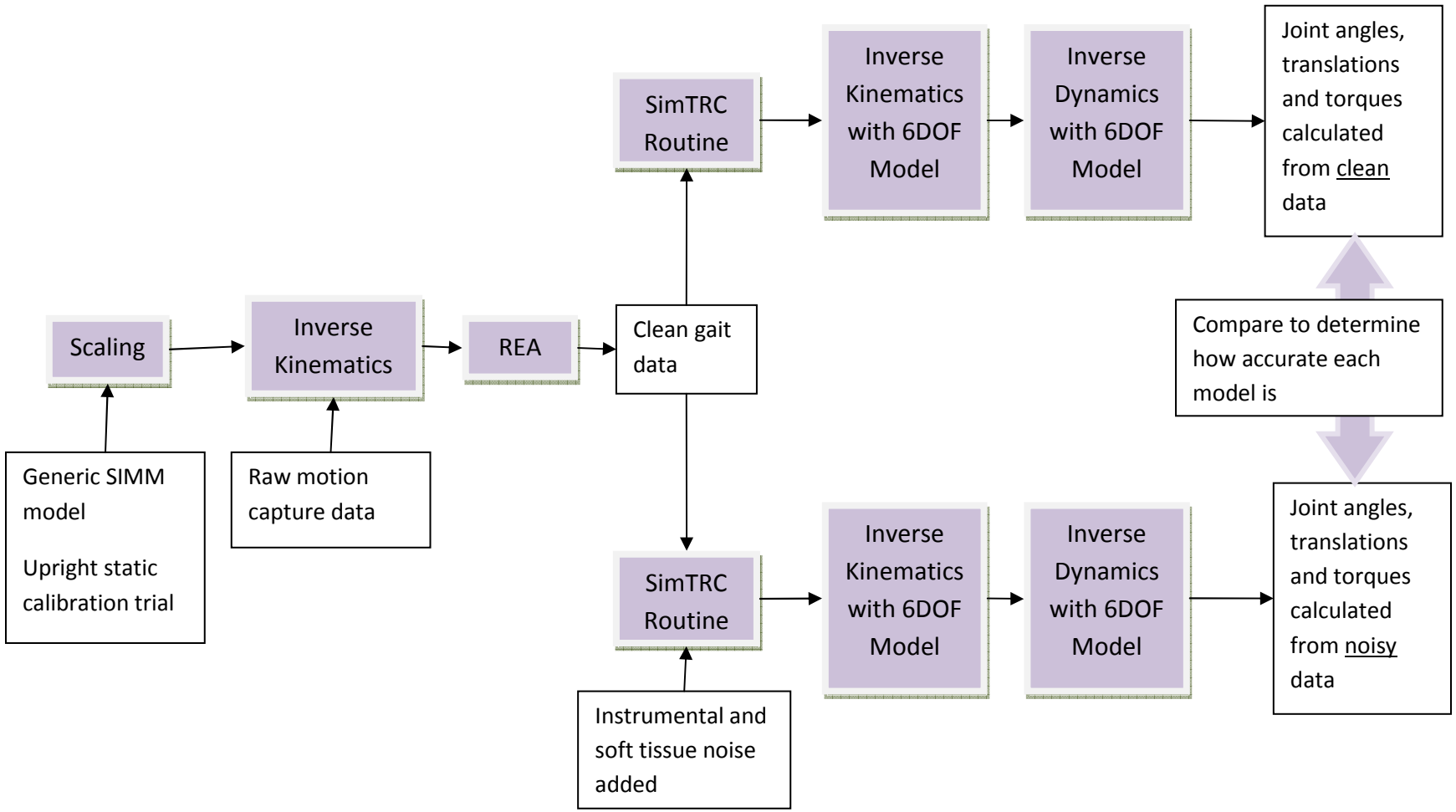

Figure 7: This chart shows the steps involved in the simulation. See text for explanation.

First, a generic musculoskeletal model was created in SIMM (SIMM4.0, Musculographics Inc.). The hip was modeled as a ball and socket with the joint center at the center of the femoral head [12]; the knee with flexion coupled kinematics [28] and the joint center between the femoral epicondyles [29]; and the ankle as two hinge joints, talocrural and subtalar joints [12]. The center of the talcrural joint was placed between the tibia/fibula malleoli [29] with an anatomically defined axis for plantar/dorsiflexion [30]. The subtalar joint was offset from the talocrural joint [12] with an anatomically defined axis for inversion/eversion [30]. The appendix summarizes various joint models used in the literature. For each segment, the x axis defined ab/adduction, y axis internal/external rotation, and z axis flexion/extension. In a neutral, upright configuration, the x axis pointed forward, the y axis upward, and the z axis to the right.

Next, the generic model was scaled using an upright calibration trial. Markers from the calibration trial were used to compute each subject's segment lengths. The average distance between a pair of markers on each segment was computed. The marker pairs for each segment are shown in the appendix. The ratio of this distance to the distance between the skeleton fixed markers of the unscaled generic model was computed and used as a segment scaling factor. Calibration markers were also used to compute joint angles that optimally fit the scaled skeleton to the anatomical marker positions measured in the calibration trial. All markers' local coordinates were then reset on the segments so the global marker positions would match identically with the measured marker positions in the calibration trial.

Then, joint angles were computed using inverse kinematics on the motion capture data. During inverse kinematics, the raw marker data was filtered at 6 Hz and the force plate data at 100 Hz. The joint angles and ground reaction forces were subsequently passed through a residual elimination algorithm (REA) to recalculate segment accelerations to be dynamically consistent with the ground reaction forces measured and reproduce the desired motion [5]. Marker data was filtered at 6 Hz and force plate data

at 100 Hz during REA. REA has been shown in partially reject noise and compensate for static offset between the force plates and motion system reference frames [5].

After the REA, clean and noisy marker trajectories were simulated. For the clean marker trajectories, no noise was added to serve as a 'ground truth'. 1 mm standard deviation of instrumental noise [25] was added to the noisy marker trajectories, along with soft tissue artifact [6]. The simulated marker trajectories were passed through inverse kinematics with a 6 degree of freedom model to calculate joint angles with the markers and force plate data filtered at 100 Hz. Two marker sets were used during the 6 degree of freedom inverse kinematics and inverse dynamics: a shared marker set (Figure 8 and Figure 9) and an independent set (Figure 6) [31]. The data was subsequently passed through inverse dynamics where the noisy markers were filtered at 6 Hz, while the clean markers were filtered at 100 Hz. Force plate data was filtered at 100 Hz regardless of noise present in marker data.

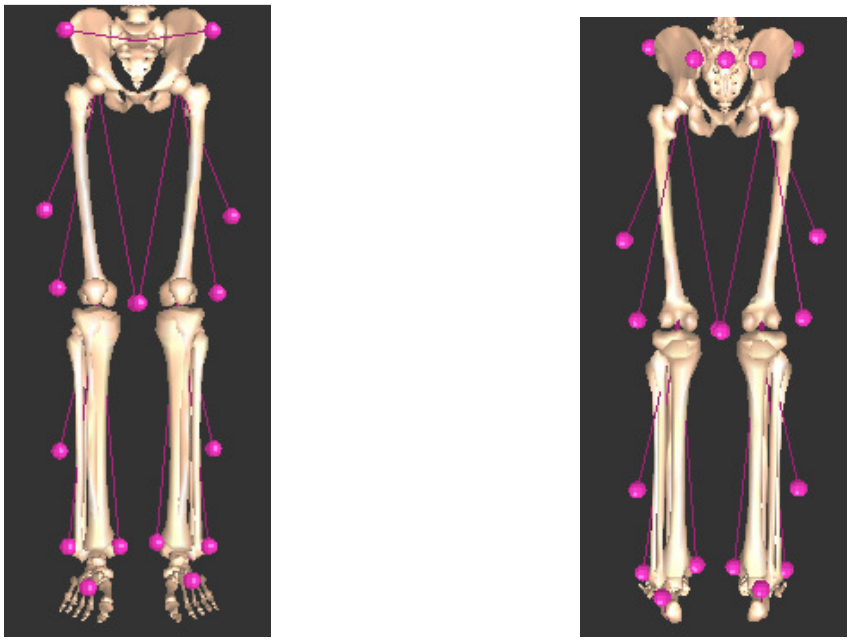

Figure 8: 18 retro reflective markers were used in the shared marker set, along with calculated hip, knee, and ankle joint centers.

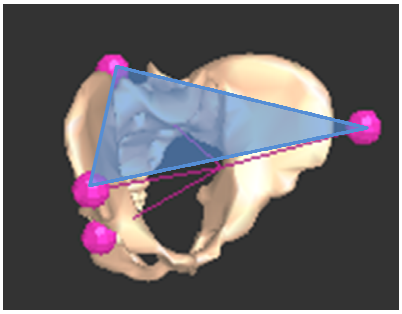

The pelvis was tracked using the RASIS, LASIS, and a marker at S2. The pelvis markers were used to calculate a virtual hip joint center.

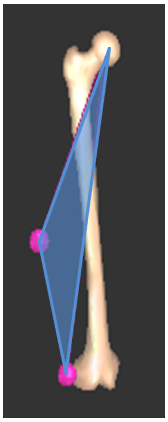

The virtual hip joint center was used in the tracking of the thigh, along with markers on the thigh and the femoral epicondyle. The thigh markers were used to calculate a virtual knee joint center.

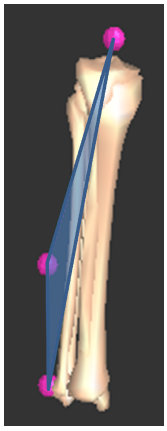

Markers on the shank, tibial epicondyle, and virtual knee joint center were used to track the shank. The shank markers were used to calculate a virtual ankle joint center.

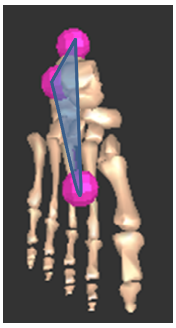

The virtual ankle joint center was used to track the foot in addition to markers on the toes and heel.

Figure 9: Motion was tracked with a shared marker set by using virtual hip, knee, and ankle joint centers, along with physical markers placed on the body.

Joint torques, angles, and translations calculated from noisy marker data and clean data that exactly recreated the gait motion were compared and RMS error calculated for both the normal and cerebral palsy subjects. For each joint variable, a two-way repeated measures ANOVA was used to assess the effects of health (normal, cerebral palsy) and model (shared, independent) on the RMS error, with Tukey's post-hoc test to assess interactions. Significance was defined as $p<0.05$.

Results

Translations

Compared to the independent marker set, the shared marker set showed lower RMS errors for all joint translations (Table 1).

Angles

When compared to a shared marker set, use of an independent marker set resulted in smaller RMS errors for hip and knee internal/external rotation angles for both the normal subjects and cerebral palsy patients and ankle internal/external rotation for the cerebral palsy patients (Table 1). The shared marker set showed lower RMS errors in hip and knee ab/adduction for both subject groups and ankle ab/adduction for the normal subjects.

Torques

The shared marker set resulted in smaller RMS errors for non-sagittal hip and knee torques for both subject groups while the independent marker set showed lower RMS errors for ankle ab/adduction torque for the cerebral palsy patients (Table 1).

Table 1: Root mean square (RMS) errors using shared and independent marker sets on each segment

	Normal		Cerebral Palsy		Significant Factors		
	Shared Marker Set	Independent Marker Set	Shared Marker Set	Independent Marker Set	Model	Health	Model*Health
Hip_A/P_translation	1.3(0.3)	12.7(3.3)	1.6(0.6)	14.8(6.5)	p<0.001		
Hip_S/I_translation	2.4(0.6)	10.2(3.0)	2.5(0.7)	10.8(3.6)	p<0.001		
Hip_M/L_translation	1.2(0.4)	17.2(6.4)	1.0(0.4)	17.5(4.7)	p<0.001		
Hip_flex_angle	3.3(0.8)	4.3(1.4)	2.9(0.6)	4.6(2.0)	p<0.001		
Hip_add_angle	1.8(0.5)	4.8(1.2)	2.3(0.6)	4.4(1.2)	p<0.001		
Hip_rot_angle	8.4(3.2)	5.3(1.7)	8.5(3.7)	5.0(1.7)	p<0.001		
Hip_flex_torque	2.4(0.6)	4.1(1.7)	3.4(1.0)	5.5(2.4)	p<0.001	p<0.05	
Hip_add_torque	3.1(1.6)	4.6(1.7)	3.5(1.6)	5.1(1.6)	p<0.001		
Hip_rot_torque	1.1(0.5)	2.2(0.9)	1.6(0.4)	2.8(1.1)	p<0.001	p<0.05	
Knee_A/P_translation	2.7(1.3)	17.8(4.6)	3.0(1.2)	15.1(4.9)	p<0.001		
Knee_S/I_translation	2.9(0.7)	9.6(3.5)	3.0(1.1)	9.5(2.6)	p<0.001		
Knee_M/L_translation	1.3(0.7)	24.9(10.1)	1.4(0.5)	15.9(5.1)	p<0.001	p<0.05	p<0.05
Knee_flex_angle	3.5(1.3)	5.4(1.8)	3.2(1.4)	5.7(1.8)	p<0.001		
Knee_add_angle	4.2(2.1)	6.8(1.6)	4.6(2.4)	5.7(1.7)	p<0.01		
Knee_rot_angle	9.6(2.5)	6.9(2.1)	11.8(7.8)	6.0(1.5)	p<0.001		
Knee_flex_torque	3.6(1.4)	4.9(2.3)	4.9(2.0)	5.2(2.6)			
Knee_add_torque	2.8(1.2)	5.7(3.1)	4.1(2.2)	5.3(3.1)	p<0.01		
Knee_rot_torque	0.5(0.2)	2.6(1.1)	0.8(0.3)	3.0(2.1)	p<0.001		
Ankle_A/P_translation	4.4(0.9)	8.9(2.1)	4.0(1.2)	10.5(2.8)	p<0.001		
Ankle_S/I_translation	0.7(0.3)	7.8(2.4)	1.2(0.6)	8.6(2.8)	p<0.001		
Ankle_M/L_translation	2.1(0.9)	12.1(4.2)	2.5(3.2)	11.6(3.2)	p<0.001		
Ankle_flex_angle	3.5(0.9)	5.9(1.9)	5.2(5.0)	6.0(1.5)			
Ankle_add_angle	3.0(1.9)	6.9(1.5)	4.5(3.0)	5.8(1.7)	p<0.001		p<0.05
Ankle_rot_angle	8.6(2.3)	6.1(1.3)	12.2(7.1)	4.4(0.7)	p<0.001		p<0.05
Ankle_flex_torque	2.5(1.0)	4.7(2.2)	6.9(6.1)	5.6(2.3)		p<0.05	p<0.05
Ankle_add_torque	6.4(3.1)	6.3(3.4)	12.5(8.1)	6.7(4.5)	p<0.05	p<0.05	p<0.05
Ankle_rot_torque	2.4(1.7)	3.0(1.1)	6.6(6.7)	5.2(3.5)		p<0.01	

Discussion

Our results suggest that the use of independent marker sets, in which 3 or more markers are placed on a rigid plate attached mid-segment, may enhance the accuracy of 3D joint angles. The most noteworthy improvements were internal-external rotation angles and likely result from using redundant non-collinear markers displaced from the long axis of the joint. However, the clusters of marker used in independent marker sets may be inaccurate in determining ab/adduction since these clusters are usually placed in the center of the segment and used to predict motion at the distal and proximal ends of the bone. Small noise errors in cluster motion may create large errors in predicted motion about the joints.

The independent marker set showed large RMS errors in joint translations. This may be due to the noise model used. Each marker was assumed to have independent soft tissue artifact. Figure 10 shows one possible movement of the plate markers assuming independent soft tissue noise. The plate markers should have noise that is in phase with each other so the entire plate would move as a single unit.

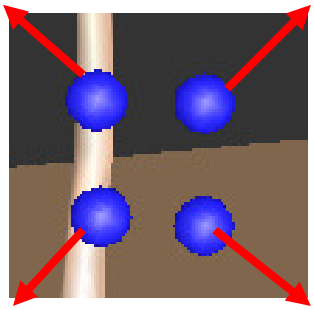

Figure 10: The plate markers were assumed to have independent soft tissue artifact, which may lead to abnormally large joint translations.

According to Reinschmidt [32], 2.4 degrees of RMS error in knee ab/adduction can be attributed to soft tissue artifact, 3.9 degrees of error in knee internal/external rotation, and 2.1 degrees of error in knee flexion. Both the shared and independent marker sets amplified this noise. Also, 3.6 degrees of

ankle ab/adduction, 3.2 degrees of internal/external rotation, and 2.2 degrees of flexion about the ankle can be attributed to soft tissue artifact [32]. Neither marker model fully rejects soft tissue noise about the ankle.

A hybrid model may be the best choice for using motion analysis in surgical planning. Marker clusters should be used to capture motion about the long-axis of the bone and joint centers to capture ab/adduction and translations.

Works Cited

1. Davis, R.B., et al., *A gait analysis data collection and reduction technique.* Human Movement Science, 1991. **10**(5): p. 575-587.
2. Leardini, A., et al., *Human movement analysis using stereophotogrammetry, Part 3: Soft tissue artifact assessment and compensation.* Gait & Posture, 2005. **21**: p. 212-225.
3. Cappozzo, A., et al., *Surface-marker cluster design criteria for 3-D bone movement reconstruction.* IEEE Trans Biomed Engr, 1997. **44**(12): p. 1165-1174.
4. Buczek, F.L., et al., *Comparing normal gait analyses using conventional and least-squares six degree-of-freedom models*, in *Gait and Clinical Movement Analysis Society*. 2005: Portland, OR.
5. Remy, C.D. and D.G. Thelen, *Optimal Estimation of Dynamically Consistent Kinematics and Kinetics for Forward Dynamic Simulation of Gait.* J Biomech Eng 2008. ( ): p. in press.
6. Cheze, L., B.J. Fregly, and J. Dimnet, *A Solidification Procedure to Facilitate Kinematic Analyses Based on Video System Data.* J Biomech, 1995. **28**(7): p. 879-884.
7. Cappozzo, A., et al., *Human movement analysis using stereophotogrammetry, Part 1: theoretical background.* Gait & Posture, 2005. **21**: p. 186-196.
8. Seidel, G.K., et al., *Hip Joint Center Location from Palpable Bondy Landmarks - A Cadaver Study.* J Biomech, 1995. **28**(8): p. 995-998.
9. Bell, A.L., D.R. Pedersen, and R.A. Brand, *A Comparison of the Accuracy of Several Hip Center Location Prediction Methods.* J Biomech, 1990. **23**(6): p. 617-621.
10. Leardini, A., et al., *Validation of a functional method for the estimation of hip joint centre location.* J Biomech, 1999. **32**: p. 99-103.
11. Schwartz, M.H. and A. Rozumalski, *A new method for estimating joint parameters from motion data.* J Biomech, 2005. **38**: p. 107-116.
12. Delp, S.L., et al., *An interactive graphics-based model of the lower extremity to study orthopaedic surgical procedures.* IEEE Trans Biomed Engr, 1990. **37**(8): p. 757-67.
13. Wu, G., et al., *ISB recommendation on definitions of joint coordinate system of various joints for the reporting of human joint motion--part I: ankle, hip, and spine.* J Biomech, 2002. **35**(4): p. 543-548.
14. Chiari, L., et al., *Human movement analysis using stereophotogrammetry, Part 2: Instrumental errors.* Gait & Posture, 2005. **21**: p. 197-211.

15. Della Croce, U., et al., *Human movement analysis using stereophotogrammetry, Part 4: assessment of anatomical landmark misplacement and its effects on joint kinematics.* Gait & Posture, 2005. **21**: p. 226-237.
16. Davis, R.B., III, *Clinical gait analysis.* IEEE Engr in Med and Biol, 1988. **7**(3): p. 35-40.
17. Whittle, M.W., *Clinical gait analysis: A review.* Human Movement Science, 1996. **15**(3): p. 369-387.
18. Anderson, F.C., et al., *OpenSim User's Guide*. 2008.
19. Subramanian, N., et al., *Gait before and 10 years after rhizotomy in children with cerebral palsy spasticity.* Neurosurg Focus, 1998. **4**(1): p. article 1.
20. Patrick, J., A. Roberts, and G. Cole, *Therapeutic choices in the locomotor management of the child with cerebral palsy - more luck than judgement?* Arch Dis Child, 2001. **85**: p. 275 - 279.
21. Koman, A., et al., *Botulinum Toxin Type A Neuromuscular Blockade in the Treatment of Equinus Foot Deformity in Cerebral Palsy: A Multicenter, Open-Label Clinical Trial.* Pediatrics, 2001. **108**: p. 1062-1071.
22. Sutherland, D.H., et al., *The development of mature gait.* J Bone Joint Surg Am, 1980. **62**(3): p. 336-353.
23. Kadaba, M.P., H.K. Ramakrishnan, and M.E. Wootten, *Measurement of lower extremity kinematics during level walking.* J Othoped Res, 1990. **8**(3): p. 383-392.
24. Spoor, C. and F. Veldpaus, *Rigid body motion calculated from spatial co-ordinates of markers.* J Biomech, 1980. **13**(4): p. 391-393.
25. Andriacchi, T.P., et al., *A point cluster method for in vivo motion analysis: applied to a study of knee kinematics.* J Biomech Eng, 1998. **120**(6): p. 743-9.
26. Winters, T.F., J.R. Gage, and R. Hicks, *Gait patterns in spastic hemiplegia in children and young adults.* J Bone Joint Surg Am, 1987. **69**(3): p. 437-441.
27. Rodda, J. and H.K. Graham, *Classification of gait patterns in spastic hemiplegia and spastic diplegia: a basis for a management algorithm.* Euro J Neuro, 2001. **8**: p. 98-108.
28. Walker, P.S., J.S. Rovick, and D.D. Robertson, *The effects of knee brace hinge design and placement on joint mechanics.* J Biomech, 1988. **21**(11): p. 965-74.
29. Cappozzo, A., et al., *Position and orientation in space of bones during movement: anatomical frame definition and determination.* Clin Biomech, 1995. **10**(4): p. 171-178.
30. Inman, V.T., *The Joints of the Ankle*. 1976, Baltimore, MD: Williams and Wilkins.

31. Buczek, F.L., et al., *Comparing normal gait analyses using conventional and least-squares optimized tracking methods*, in *International and Americal Societies of Biomechanics*. 2005: Cleveland, OH.

32. Reinschmidt, C., et al., *Tibiofemoral and tibiocalcaneal motion during walking: external vs. skeletal markers.* Gait & Posture, 1997. **6**(2): p. 98-109.

33. Piazza, S.J., et al., *Assessment of the functional method of hip joint center location subject to reduced range of hip motion.* Journal of Biomechanics, 2004. **37**(3): p. 349-56.

34. Wu, G., et al., *ISB recommendation of definitions of joint coordinate system of various joints for the reporting of human joint motion - part 1: ankle, hip, and spine.* J Biomech, 2002. **35**: p. 543-48.

35. Cappozzo, A., et al., *Position and orientation in space of bones during movement: anatomical frame definition and determination.* Clin Biomech (Bristol, Avon), 1995. **10**(4): p. 171-178.

36. Hagemeister, N., et al., *A reproducible method for studying three-dimensional knee kinematics.* Journal of Biomechanics, 2005. **38**: p. 1926-31.

37. Siston, R., et al., *Evaluation of Methods That Locate the Center of the Ankle for Computer-assisted Total Knee Arthroplasty.* Clin Orthop and Related Research, 2005. **439**: p. 129-35.

38. Demarais, D., R. Bachschmidt, and G.F. Harris, *The Instantaneous Axis of Rotation (IAOR) of the Foot and Ankle: A Self-Determining System With Implications for Rehabilitation Medicine Application.* IEEE Trans Neural Syst Rehabil Eng, 2002. **10**(4): p. 232-238.

Appendices

Joint Models of the Hip, Knee, and Ankle

Generic musculoskeletal models can employ many simplified joint models. Table 2 through Table 4 summarizes common joint models used in the literature.

Table 2: Hip Joint Models

Hip Joint Center Location	Methods	Joint Coordinate System	Source
1.5 – 2 cm directly distal to midpoint of a line between pubic symphosis and ASIS in frontal plane projection; directly medial to greater trochanter in sagittal plane	Actual hip center from radiographs; Total error: 3.61 cm +- 1.2 cm	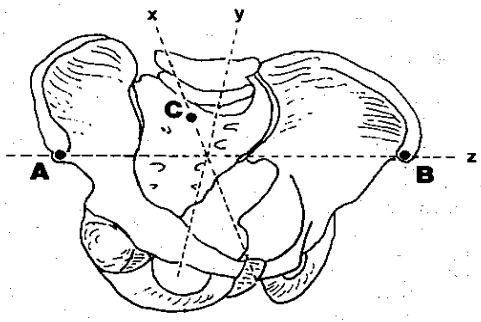 Fig. 1. Pelvic marker reference frame. Defined by markers over the right ASIS (Point A), the left ASIS (point B), and the midpoint between the PSISs (point C). The mid-PSIS marker is behind the sacrum, and would not normally be visible in this view.	Andriacchi from [9]
19% of inter-ASIS distance posterior, 30% distal, and 14% medial to ASIS	Actual hip center from radiographs; 1.90 cm +- 1.2 cm		Tylkowski from [9]
Rotational method	Actual hip center from radiographs; 3.79 cm +- 1.9 cm		[9]
Relative to ASIS: 14% of pelvic width (ASIS to ASIS) medially (0.58 cm error); 34% of pelvic depth (ASIS to PSIS) posterior (0.30 cm error); 79% of pelvic height (perpendicular from pubic center to inter-ASIS line) inferior (0.35 cm error)	Cadaver study	The frontal plane was defined as the plane passing through both ASISs and the pubic symphysis. The coordinate system was defined with its origin at the respective ASIS side being measured: y-axis mediolateral (positive medial-defined by ASISs), z-axis superoinferior (positive inferior), and x-axis anteroposterior (positive posterior).	[8]

Functional method (13 mm average error). When range of motion reduced, 26 mm error [33]	True HJC found with roentgen stereophotogrammetric analysis. To find the HJC, the subject performed continuously and sequentially a flexion-extension followed by abd/adduction of right hip. Next, cycle of ihp circumduction. HJC estimated as the center of the optimal spherical surface that fitted the trajectory of the thigh marker centroid.	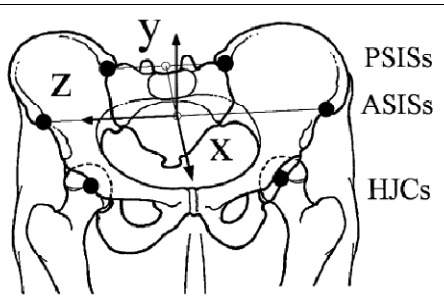 Fig. 1. Pelvic anatomical landmarks and anatomical frame. The origin was selected at the midpoint between the right and left ASIS. The *z*-axis was oriented as the line passing through the ASISs with its positive direction from left to right. The *x*-axis lay in the quasi-transverse plane defined by the ASISs and the midpoint between the PSISs and with its positive direction forwards. The *y*-axis was orthogonal to the *xz*-plane and its positive direction was proximal (Cappozzo et al., 1995a).	[10]
Functional method (varies 1 – 3 mm between subjects) (i) the motions of two adjacent segments spanning a single joint are tracked, (ii) the axis of rotation between every pair of observed segment configurations is computed, (iii) the most likely intersection of all axes (effective joint center) and most likely orientation of the axes (effective joint axis) is found	Motion capture.	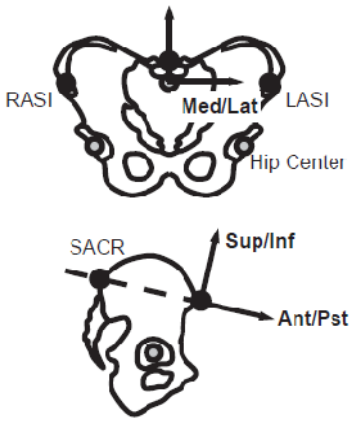	[11]

-	-	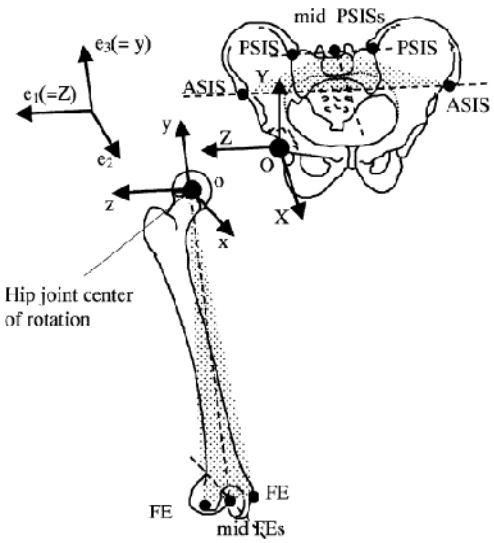 mid PSISs PSIS PSIS ASIS ASIS e3(= y) e1(=Z) e2 Y y Z O o z x X Hip joint center of rotation FE FE mid FEs	[34]
-	-	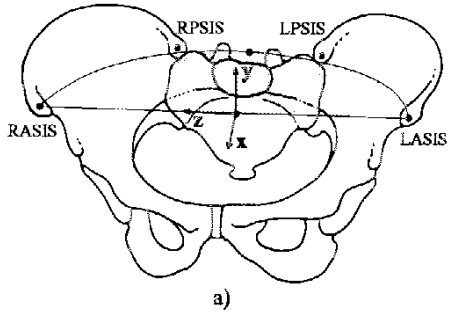 RPSIS LPSIS y z x RASIS LASIS a)	[35]

Table 3: Knee Joint Models

Knee Joint Center Location	Methods	Joint Coordinate System	Source
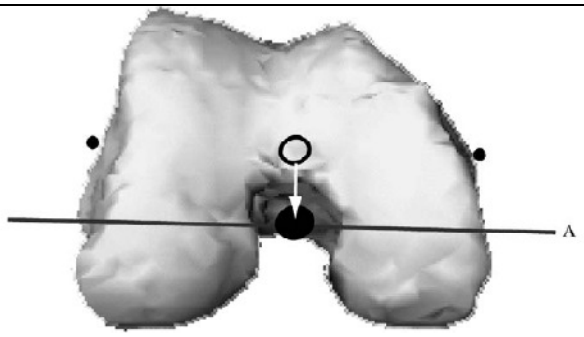 Fig. 3. Knee joint center (filled circle) is defined as the mid-point (empty circle) between the femoral epicondyles (dots) projected onto the mean flexion axis (A) calculated during flexion/extension movement.	Motion capture	Functional and postural: Longitudinal axes connect hip and knee for thigh JCS and knee and ankle for shank JCS. Flex/extend knee to find ant/pos axes.	[36]
Functional method. (i) the motions of two adjacent segments spanning a single joint are tracked, (ii) the axis of rotation between every pair of observed segment configurations is computed, (iii) the most likely intersection of all axes (effective joint center) and most likely orientation of the axes (effective joint axis) is found	Motion capture.	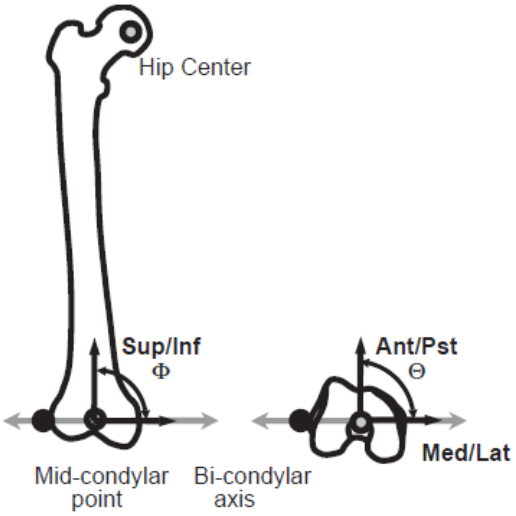	[11]
Between epicondyles.	-	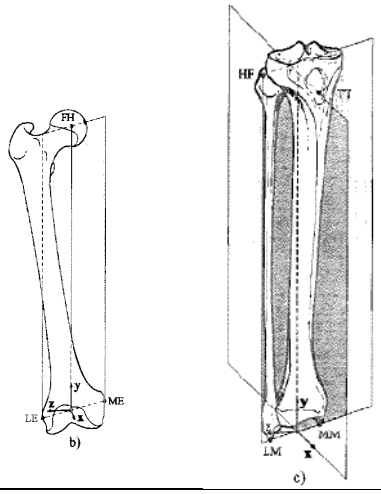	[35]

Table 4: Ankle Joint Models

Ankle Joint Center Location	Methods	Joint Coordinate System	Source
Ankle center is centered between malleoli.	MRI images.	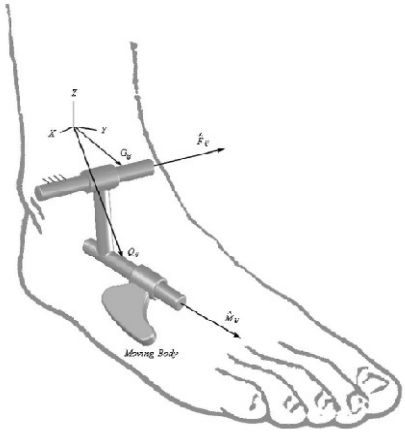 Fig 6. The location and orientation of the fixed and moving axes are identified with respect to the tibia reference frame in this biaxial ankle model.	[37]
Centered between malleoli.	Motion capture.	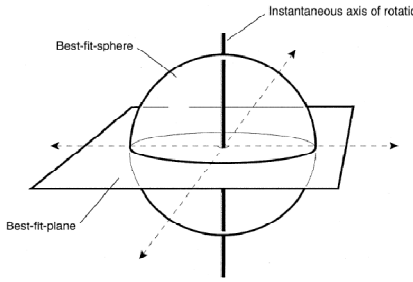 Fig. 2. A plane and sphere fit to marker trajectories with the constraint that the sphere center lie on the plane. The IAOR was defined perpendicular to the plane and passing through the center of the sphere.	[38]
Between malleoli.	-	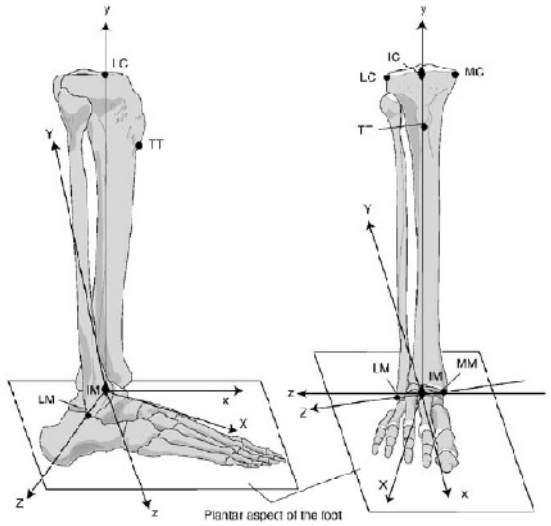 Fig. 1. Illustration of the tibia/fibula coordinate system (*XYZ*) and the calcaneus coordinate system (*xyz*) with the ankle joint complex in the neutral position.	[34]
Between malleoli.	-	See picture in knee table	[35]

Scaling Rules

Segment scaling markers are used to compute segment lengths. The average distance between each pair of markers is computed for both the generic model and upright standing calibration trial. The ratio between these distances in the generic model and calibration trial is used as a scaling factor in the segment's x, y, and z directions. Table 5 shows the scaling rule used for each segment.

Table 5: Scaling rules used for each segment

Segment to be scaled	**Distances averaged to compute scaling ratio**	**Picture**
Pelvis Femur Patella	Distance 1 = between right anterior superior iliac spine and right lateral femoral epicondyles Distance 2 = repeat for left side	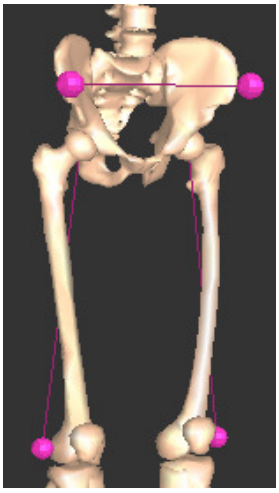
Tibia Talus	Distance 1 = between right lateral femoral epicondyles and right lateral malleolus Distance 2 = repeat for left side	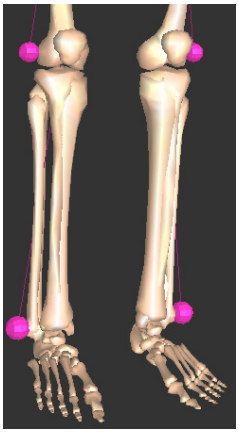

Foot Toes	Distance 1 = between right anterior superior iliac spine and right lateral femoral epicondyles Distance 2 = repeat for left side Distance 3 = between right lateral femoral epicondyles and right lateral malleolus Distance 4 = repeat for left side	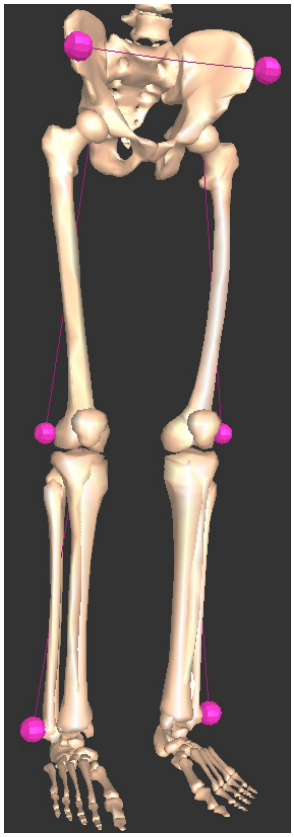
Torso Neck and Head	Distance 1 = between right anterior superior iliac spine and right articular acromioclaviculare Distance 2 = repeat for left side	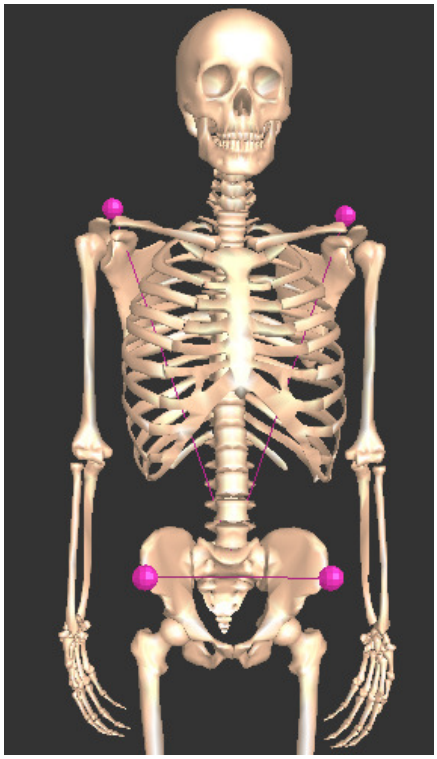

<table>
<tr><td>Humerus</td><td>Distance 1 = between right articular acromioclaviculare and right lateral epicondyle of humerus

Distance 2 = repeat for left side</td><td> 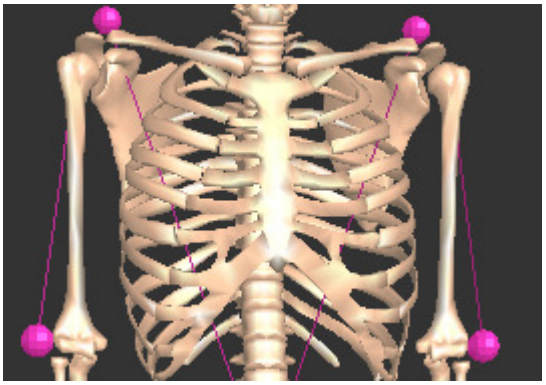 </td></tr>
<tr><td>Ulna

Radius</td><td rowspan="2">Distance 1 = between right lateral epicondyle of humerus and radial styloid

Distance 2 = repeat for left side</td><td rowspan="2">  </td></tr>
<tr><td>Hand</td></tr>
</table>

Resume

OBJECTIVE: I would like to use computer simulations to optimize surgical techniques used to improve gait performance.

QUALIFICATIONS

○ Experience with 3D Motion Analysis software (EVaRT, SIMM, Visual3D, OpenSim), Matlab, Statistica, Unigraphics, SolidWorks, Finite Element Analysis software (ANSYS and ABAQUS), Microsoft Office, GeoMagic, ProEngineer, AutoCAD, Instron testing machines, LabView
○ Experience with technical writing, presentations, teamwork, and design work
○ Conversation and culture skills in Spanish

EDUCATION

1998-2002 High School Graduate, Fond du Lac High School
Cumulative GPA 3.85, Class Rank 21 of 584 (top 4.0 %)

2002-2006 B.S. from UW Madison in Mechanical Engineering with Research Honors, Cumulative GPA 3.883, Class Rank 33 of 671 (top 5.0 %)

2007-present M.S. student at UW Madison in Biomedical Engineering
Cumulative GPA 4.0

EXPERIENCE

Jan. 2007 – present Research Assistant with Darryl Thelen, Biomechanics, UW Madison Biomed. Engr. Dept. – Part Time

I worked with electromyography traces of young and old subjects to investigate whether biomechanical adaptations in muscles or neuromuscular adaptations are dominant. I also worked on a sensitivity analysis of motion data. We introduced noise into the motion data of markers placed on a subject and investigated whether more markers reduced the effect of noise when the motion data was used to calculate kinetics and kinematics of gait.

May 2006 – Aug. 2006 Mechanical Engr. Co-op, General Electric – Full Time

My main project was to assist in the design development of an ultrasound guided needle-positioning mechanism for regional anesthesia. I obtained specifications from a clinician and used his feedback for product design iterations. I also performed a tolerance analysis of a locking mechanism on an anesthesia chemical vaporizer that enables only one drug at a time to be administered to a patient. I helped to incorporate a new product, a MicroOptical Heads Up Display Device, into GE's documentation and purchasing system. Another project of mine was to tested optical properties and response time of a silica gel that turns green when moisture is present in air flow.

Aug. 2005 – Dec. 2006 Research Assistant with Heidi Ploeg, Biomechanics, UW Madison Mech. Engr. Dept. – Part Time

My research project was working with a prosthetic foot for land mine victims. I used data obtained from a laser scan of the prosthetic foot to produce a solid 3D computer model, run a finite element analysis on the model to predict failure loads and points of fracture, and mechanically test a prototype of the foot. My thesis compared the finite element stiffness testing results and mechanical testing results to determine a valid mechanical testing method that can be simulated in a finite element analysis.

May 2005 – Aug. 2005 Mechanical Engr. Co-op, Kimberly Clark – Full Time
My main project was to design a vacuum system for a production machine, order parts for the system, support installation, provide accurate documentation and drawings, and troubleshoot upon startup. Upon the completion of my term, I did a final presentation for my team on what I had designed.

Aug.2004 – Jan. 2005 Mechanical Engr. Co-op, Environmental Health – Full Time
My main project was to redesign a fume hood exhaust system for Engineering Hall on campus. I also certified fume hoods and biological safety cabinets, designed a sound attenuation system for an office on campus, and wrote a cost analysis on fume hood energy consumption.

COMMUNITY AND EXTRACIRICULAR

- Member of the UW Center for Rehabilitation Engineering and Assistive Technology
- Volunteer for the Dane County Human Society as a Canine Companion
- Member of National Society of Collegiate Scholars
- Member of Tau Beta Pi Engineering Honor Society
- Dean's Honor List – Fall 2002 to present
- Nora Adams Scholarship 2004
- Professor Elliot Scholarship 2004
- National W Club Scholarship 2002, 03, 04
- Hilldale Research Fellowship 2006
- Gustav A. Rehm Memorial Scholarship – 2006
- Faustin Prinz Scholarsip – 2006
- UW Madison Engr. Undergraduate Scholarship from the Dept. of Mechanical Engr. 2002,03
- National Science Foundation Fellowship Honorable Mention 2006
- UW Madison Institute on Aging Predoctoral Fellowship 2008

PUBLICATIONS AND PRESENTATIONS

Baus, A. (2006) *Validation of a Prosthetic Foot Stiffness Testing Procedure*. (poster and abstract presented at the UW Madison Undergraduate Symposium). Madison: University of Wisconsin Madison Bone and Joint Biomechanics Lab.

Schmitz, A. (2007) *Stiffness Analyses for the Design Development of a Prosthetic Foot.* (undergraduate thesis). Madison: University of Wisconsin Madison Wendt Library.
Available at: http://digital.library.wisc.edu/1793/11505

Schmitz. A. (2006) *Validation of a Prosthetic Foot Stiffness Testing Procedure.* (poster presented at the UW Rehabilitation Expo). Madison: University of Wisconsin Madison Bone and Joint Biomechanics Lab.

Schmitz, A. M., Ploeg, E. L., Beshai, L. M., Bryant, J. T., Ploeg, H.. (2007) *Stiffness Analyses for the Design Development of a Prosthetic Foot*. (poster and abstract presented at 12th World Congress of the International Society for Prosthetics and Orthotics). Vancouver: 12th World Congress of ISPO.

Schmitz, A., Silder, A., Heiderscheit, B., Mahoney, J., Thelen, D. (2007) *Neuromuscular and Biomechanical Adaptations in Aging Leg Muscles* (poster and abstract presented at the 19th Colloquium on Aging). Madison: University of Wisconsin Madison Neuro-musculoskeletal Research Lab.

Schmitz, A., Silder, A., Heiderscheit, B., Mahoney, J., Thelen, D. (2008) *Differences in Lower-Extremity Muscular Activation during Walking Between Healthy Older and Young Subjects*. In press. Journal of Electromyography and Kinesiology

Schmitz, A., Silder, A., Heiderscheit, B., Mahoney, J., Thelen, D. (2008) *Age Related Changes in the Neuromuscular Coordination of Human Walking* (podium presentation at the Fourth North American Congress on Biomechanics). Ann Arbor, Michigan: NACOB.